Brain Structure and Function (2019) 224:1505–1518
https://doi.org/10.1007/s00429-019-01845-5

ORIGINAL ARTICLE

Optogenetic stimulation of basal forebrain parvalbumin neurons modulates the cortical topography of auditory steady-state responses

Eunjin Hwang[1] · Ritchie E. Brown[2] · Bernat Kocsis[3] · Tae Kim[4] · James T. McKenna[2] · James M. McNally[2] · Hio-Been Han[1,5] · Jee Hyun Choi[1,6]

Received: 8 May 2018 / Accepted: 6 February 2019 / Published online: 2 March 2019

Abstract

High-density electroencephalographic (hdEEG) recordings are widely used in human studies to determine spatio-temporal patterns of cortical electrical activity. How these patterns of activity are modulated by subcortical arousal systems is poorly understood. Here, we couple selective optogenetic stimulation of a defined subcortical cell-type, basal forebrain (BF) parvalbumin (PV) neurons, with hdEEG recordings in mice (Opto-hdEEG). Stimulation of BF PV projection neurons preferentially generated time-locked gamma oscillations in frontal cortices. BF PV gamma-frequency stimulation potently modulated an auditory sensory paradigm used to probe cortical function in neuropsychiatric disorders, the auditory steady-state response (ASSR). Phase-locked excitation of BF PV neurons in advance of 40 Hz auditory stimuli enhanced the power, precision and reliability of cortical responses, and the relationship between responses in frontal and auditory cortices. Furthermore, synchronization within a frontal hub and long-range cortical interactions were enhanced. Thus, phasic discharge of BF PV neurons changes cortical processing in a manner reminiscent of global workspace models of attention and consciousness.

Keywords Basal forebrain · Parvalbumin · Gamma oscillations · Auditory steady-state response (ASSR) · Optogenetic high-density EEG

Introduction

Ever since the invention of the electroencephalogram (EEG) by Berger almost 100 years ago (Berger 1929), scientists have been interested in the changes in cortical electrical activity which occur under different behavioral states and in response to sensory stimuli. The ability to record EEG across the scalp using high-density EEG (hdEEG) recordings in humans has further expanded this capability, allowing the analysis of spatio-temporal patterns of activity and how they are altered in particular disease states. However, human studies have a limited ability to reveal how subcortical arousal systems modulate these spatio-temporal patterns. Here, for the first time, using custom hdEEG arrays designed for mice (Choi et al. 2010) we reveal the spatio-temporal

Eunjin Hwang and Ritchie E. Brown are the first authors.

Electronic supplementary material The online version of this article (https://doi.org/10.1007/s00429-019-01845-5) contains supplementary material, which is available to authorized users.

✉ Jee Hyun Choi
jeechoi@kist.re.kr

[1] Center for Neuroscience, Korea Institute of Science and Technology (KIST), Hwarang-ro 14-gil 5, Seongbuk-gu, Seoul 02792, South Korea

[2] Department of Psychiatry, VA Boston Healthcare System and Harvard Medical School, West Roxbury, MA 02132, USA

[3] Department of Psychiatry, Beth Israel Deaconess Medical Center, Harvard Medical School, Boston, MA 02215, USA

[4] Department of Biomedical Science and Engineering, Gwangju Institute of Science and Technology (GIST), 123 Cheomdangwagi-ro C9-323 (Dasan Bldg), Buk-gu, Gwangju 61005, South Korea

[5] Program of Brain and Cognitive Engineering, Korea Advanced Institute of Science and Technology, Daejeon 34141, South Korea

[6] Division of Biomedical Science and Engineering, KIST School, University of Science and Technology, Hwarang-ro 14-gil 5, Seongbuk-gu, Seoul 02792, South Korea

patterns of cortical activity generated by selective optogenetic stimulation of a particular subcortical cell-type, basal forebrain (BF) cortically projecting parvalbumin (PV) neurons.

Our focus here is on gamma band oscillations (GBO, 30–80 Hz or higher with a resonance peak at ~ 40 Hz). Cortical GBO participate in sensory perception, attention and working memory by coordinating activity within and between cortical regions involved in different aspects of the same task (Crone et al. 2001; Fries 2009). Substantial work suggests that cortical GBO play a role in *binding* of sensory information (Gray and Singer 1989), a process involved in conscious perception. In the auditory system, GBO induced by trains of 40 Hz acoustic stimuli (auditory steady-state response, ASSR) show reduced power and phase-locking in patients with schizophrenia, in both auditory and frontal cortices (Kwon et al. 1999; O'Donnell et al. 2013; Thune et al. 2016). Furthermore, similar changes are seen in subjects who are at high risk of developing this disease (Hong et al. 2004). ASSR abnormalities correlate with positive symptoms (Spencer et al. 2008, 2009) suggesting they are functionally important markers of impaired information processing. GBO induced by visual or auditory stimuli can be modulated by attention (Tiitinen et al. 1993; Skosnik et al. 2007) via an action of frontal cortices on sensory cortices (Gregoriou et al. 2009; Schadow et al. 2009). Thus, enhancing this frontal control might be an important way to mitigate deficient GBO in schizophrenia and other disorders. However, currently we have a limited understanding of the neural systems which modulate the interaction of frontal and sensory cortices.

Most basic science work on GBO has focused on cortical mechanisms. Optogenetic and cell-type-specific molecular studies demonstrated the key role of cortical fast-spiking interneurons which contain PV (Cardin et al. 2009; Sohal et al. 2009; Korotkova et al. 2010; Carlen et al. 2012). However, cortical GBO are also modulated by ascending subcortical systems (Munk et al. 1996; Brown et al. 2012). Recently, we showed that cortically projecting BF PV neurons, the majority of which are GABAergic (McKenna et al. 2013), modulate cortical GBO, likely by synchronizing the activity of cortical PV interneurons (Kim et al. 2015). Here, we use hdEEG recordings in mice coupled with selective optogenetic stimulation, to determine the cortical topography of oscillations produced by stimulation of BF PV neurons for the first time and to examine how activity of this system modulates the spatial–temporal pattern of gamma oscillation responses produced by the ASSR paradigm which is widely used in clinical studies of schizophrenia.

Materials and methods

Animals

All the experimental procedures were approved by the Institutional Animal Care and Use Committee of the Korea Institute of Science and Technology (Permit number: 2014-027) and were performed according to the guidelines of the Korean Animal and Plant Quarantine Agency (Publication no. 12512, partial amendment 2014), as well as United States National Institute of Health guidelines (NIH publication no. 86-23, revised 1985). The experiments in this study used mice which selectively express the bacterial enzyme Cre recombinase in PV-positive neurons (B6;129P2-Pvalb$^{tm1(cre)Arbr}$/J, Stock #008069, The Jackson Laboratory, Bar Harbor, ME, USA). Experiments used adult male mice (> 10 weeks of age, body weight 25–30 g), and all efforts were made to minimize the pain or distress caused by the experiments. Animals were maintained on a 12:12 light–dark cycle (lights on at 8 AM) with food and water freely available. To ensure consistency of the results, stringent inclusion/exclusion criteria were used. The data presented in this manuscript represents a detailed analysis of the responses in five mice which had: (1) extensive viral transduction in BF, in PV neurons; (2) correct localization of the optical fiber in the MCPO region of BF; and (3) successful implantation of low impedance hdEEG arrays onto the skull. Mice were analyzed for brain mapping in response to optogenetic stimulation of BF PV neurons either alone or together with trains of auditory stimuli given at 40 Hz. Mice which did not show auditory evoked potentials were excluded from the ASSR analysis. Mice were also excluded if the hdEEGs showed high impedance in the prefrontal cortex after implantation. Mice with optical fibers located outside BF or those lacking viral transduction did not show an EEG GBO response.

Surgery

Animals were anesthetized with a ketamine-xylazine cocktail (120 and 6 mg/kg, respectively) and fixed in a stereotaxic apparatus (Model 900, David Kopf Instruments, Tujunga, CA, USA) for viral vector injection and electrode implantation. For all the experiments, we targeted the ventral, intermediate portion of the BF, including the magnocellular preoptic nucleus where we previously found the highest density of PV neurons (McKenna et al. 2013). One microliter of adeno-associated viral vector expressing channelrhodopsin2 (AAV5-DIO-EF1a-hChR2[H134R]-EYFP, University of North Carolina Vector Core, NC, USA) was injected into the left BF (AP, 0.0 mm; ML, 1.6 mm; DV, 5.5 mm) at 30 nl/min flow rate using a syringe pump (Fusion 100, Chemyx, Stafford, TX, USA). A 33-gauge needle (C315I-SPC,

Plastics One, Roanoke, VA, USA) connected to a 10 µl Hamilton syringe (#84853, Hamilton Company, Reno, NV, USA) was used for the injection, and the needle was left in place for an additional 20 min to allow for diffusion of the viral vector. After slowly removing the needle, a custom-made fiber optic cannula (200/225 µm core/clad diameter and NA = 0.39, average light transmission rate of 70%, FT200EMT, Thorlabs Inc., NJ, USA) with 1.25 mm ceramic ferrule (multimode, 230 µm inner diameter, Precision Fiber Products Inc., CA, USA) was inserted into the same site and then a 40-channel high-density microarray electrode was placed onto the skull, as previously described (Choi et al. 2010; Lee et al. 2011). We used 34 channels for this study (see Supplementary Methods). The fiber optic cannula and the microarray electrode were fixed with dental cement (Vertex Self-Curing, Vertex Dental, Zeist, Netherlands) for later stimulation and recording. After surgery, the mice were allowed to recover for 3–4 weeks before experiments began.

Opto-hdEEG

Opto-hdEEG is a method which combines optogenetic stimulation with high-density EEG for brain mapping in freely behaving mice. Microarray EEG probes were implanted over the skull of PV-Cre mice according to previously described protocols (Choi et al. 2010; Lee et al. 2011). High-density 34-channel EEG was recorded simultaneously with optogenetic BF PV stimulation given in the presence or absence of auditory stimuli. Reference and ground electrodes were positioned on the interparietal bone.

Prior to EEG recording, mice were connected to a microarray connector and a patch cable and put in 500-ml glass beaker located in a sound-proof chamber. Mice had at least 10 min of habituation period before stimulation. During the stimulation and EEG recording, mice behavior was video-recorded. For most of the stimulation time, mice were quiet and awake; stimulation trials contaminated by abrupt movement artifact (percentage of which was approximately 25% of all) were visually screened and excluded from the EEG analyses.

A block of optogenetic stimulation was composed of pulse trains delivered at six frequencies (2, 10, 20, 30, 40 and 50 Hz) in a randomly shuffled order. Sixty blocks of optogenetic stimulation were administered for each mouse. The duration of a pulse train was 5 s, the inter-train interval was 10 s, and the pulse width was 10 ms. Light intensity at the tip of the patch cable was 1.2 mW (measured by PM100D, Thorlabs, Inc., Newton, NJ, USA).

The light was delivered to the fiber optic cannula implanted to the mouse through a custom-made patch cable connected to a 470-nm LED (M470F1, Thorlabs Inc., Newton, NJ, USA), which was operated by an LED driver (DC2100, Thorlabs Inc., Newton, NJ, USA). Control signals were generated with a custom-made Matlab (MathWorks, Natick, MA, USA) program and fed to the external trigger port of the LED driver through a DAQ analog output module (#9263, National Instruments, Austin, TX, USA). The patch cable was composed of an optical connector Lucent ceramic ferrule with 1.25 mm OD at one end, an SMA-type connector at the other end, and a 1-m-long optic fiber (200/225 µm core/clad diameter and NA = 0.39, FT200EMT, Thorlabs Inc., Newton, NJ, USA) in-between. The optical connector end of the patch cable was tightly coupled to the ferrule of the implanted fiber optic cannula by a ceramic split sleeve (1.25 mm ID, 6.60 mm length, Precision Fiber Products Inc., CA, USA), and the coupling was made 20 min before the experiment. EEG signals were acquired at 2 kHz sampling rate using Synamps2 amplifier and SCAN 4.5 data acquisition system (Neuroscan, Inc., El Paso, TX, USA) and band-pass filtered between 0.1 Hz and 100 Hz.

Time-dependent stimulation of auditory steady-state stimuli

Auditory stimulation was given as trains of repetitive click sound at frequencies of 10, 20, 30, 40 and 50 Hz in a randomly shuffled order. One hundred blocks of stimulation were given to each mouse and the recording was performed twice. The duration of a click sound pulse train was 1 s, the inter-train interval was 2 s, and the pulse width was 1 ms. The fidelity of a 1-ms light pulse in activating PV neurons and producing gamma oscillations was shown by Cardin et al. (2010, Figs. 2b, 3b). Auditory stimuli (85 dB) were delivered through two pairs of personal computer speakers (signal to noise ratio ≥ 80 dBA, input impedance 10 kΩ, input sensitivity 250 ± 50 mV, frequency response 150 Hz-20 kHz, model BR-coupe, Britz International, Paju, South Korea). During the auditory stimulation, optogenetic stimulation was time-shifted in relation to the phase of auditory stimulation in four different conditions: *advanced, in-phase, delayed and out-of-phase* intervention conditions. In the *advanced* condition, a pulse of light was given earlier than the following pulse of sound by a quarter of the inter-stimulus period. In the *in-phase* condition, a pulse of sound and a pulse of light were given at the same time. In the *delayed* condition, a pulse of light was given later than the preceding pulse of sound by a quarter of the stimulation period. In the *out-of-phase* condition, the pulses of light were given in the middle of the inter-stimulus period. The frequency of optogenetic stimulation was the same as the frequency of auditory stimulation. The pulse width of light was 1 ms, and light intensity at the tip of patch cable was 1.2 mW. For the analyses presented here, steady-state auditory stimulation at 40 Hz was used.

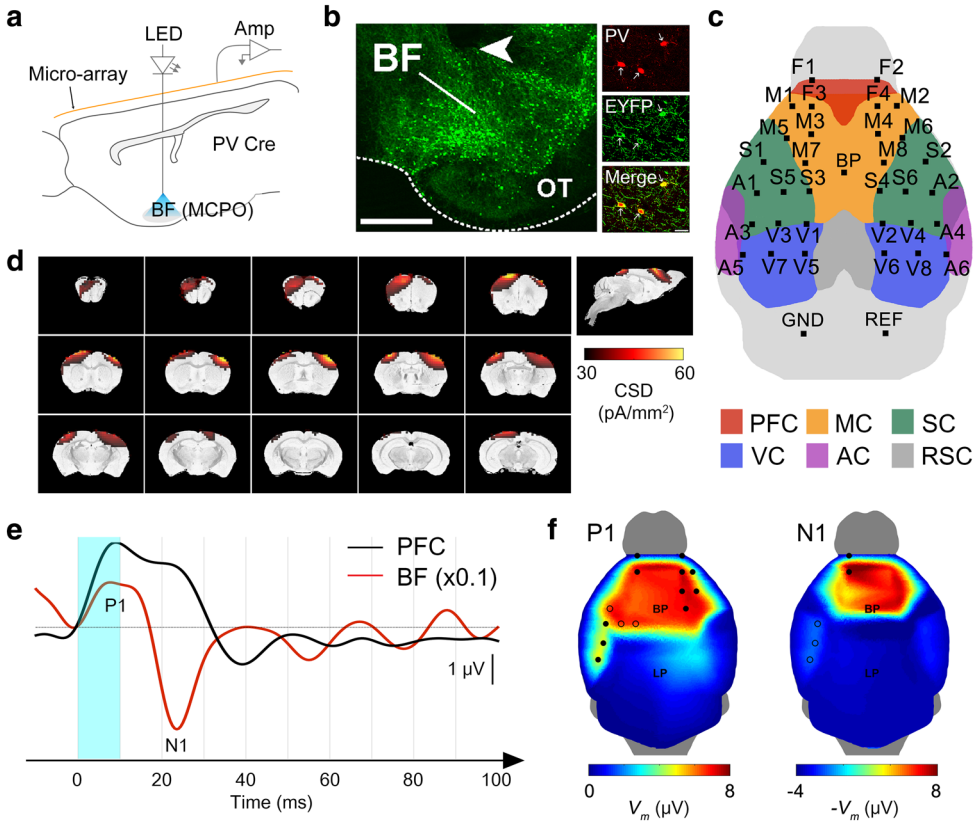

Fig. 1 Cortical brain mapping of single-pulse stimulation of BF PV neurons performed by the opto-hdEEG technique. **a** Schematic diagram of the experiment. Viral vectors carrying ChR2-EYFP were injected into the left BF of PV-Cre mice to induce selective ChR2-EYFP expression in BF PV neurons. Optical stimulation of BF PV neurons and simultaneous high-density EEG (hdEEG) recordings using microarray electrodes followed 3–4 weeks later. **b** Confirmation of viral transduction in BF PV neurons using immunohistochemistry. Tip position of the optic fiber is marked with a white arrowhead in the left panel and scale bar is 250 μm. PV immunohistochemistry (red fluorescence, top right) shows that ChR2-EYFP (green, middle right) was expressed in BF PV neurons (merged image, bottom right). Scale bar is for 20 μm. *BF* basal forebrain, *OT* olfactory tubercle. **c** Electrode montage for mouse hdEEG. The colormap of cortical areas was constructed based on the Mouse Brain in Stereotaxic Coordinates (Franklin and Paxinos 2008). *PFC* prefrontal cortex, *MC* motor cortex, *SC* somatosensory cortex, *VC* visual cortex, *AC* auditory cortex, *RSC* retrosplenial cortex, *GND* ground, *REF* reference. See also Table S1 for electrodes' coordinates. **d** Region-specific cortical activation by single-pulse stimulation of BF PV neurons. Equivalent dipoles generating surface potentials were identified by current source density (CSD) maps, estimated using averaged evoked potentials of 6369 trials, 10–30 ms after the stimulus onset. **e** Representative stimulus-locked potentials in PFC and BF (average from one mouse). Biphasic responses were observed in PFC, comprised of positive (P1) and negative (N1) deflections in succession. Peaks corresponding to P1 (0–15 ms) and N1 (15–30 ms) were fit to a Rayleigh function, $V(s) = V_m s e^{\frac{1-s^2}{2}} \left(s = \frac{t}{\tau}\right)$, to determine significant responses. **f** Topographic maps of the response amplitude (V_m) estimated from the Rayleigh model. Channels with significant activation ($p < 0.05$, Wilcoxon rank-sum test comparing V_m to basal amplitude fluctuations, see Supplementary Method for details) were marked with filled black circles and channels with marginal activation ($0.05 < p < 0.10$, Wilcoxon rank-sum test) were marked with empty circles. The response amplitude V_m for N1 peak was sign-reversed compared to P1. Non-significant regions are shaded with gray

EEG source estimation

EEG source estimations (Fig. 1d) were performed using CURRY software (ver 7, Neuroscan Inc., Herndon, VA). To reconstruct the equivalent dipole sources of the measured EEG, we built a volume conduction model with boundary element method using images downloaded from the open database of the Magnetic Resonance Microimaging Neurological Atlas Group (http://brainatlas.mbi.ufl.edu/Database). Averaged magnetic resonance images based on the C57BL/6J mouse atlas database were used for the model. Details of the volume conduction model were described in the work of Lee et al. (2013b) and a Matlab-based toolbox is available in FieldTrip (http://www.fieldtriptoolbox.org/tutorial/mouse_eeg). For the response to single-pulse stimulation, EEG traces between 15 and 30 ms after light onset were averaged over all trials and used for dipole fitting. For repetitive optogenetic stimulation, EEG traces during the stimulation period were averaged over the trials at a particular stimulation frequency.

The source was estimated with eLORETA algorithm and time-averaged source strength was superimposed with the MRI.

Analysis of single-pulse stimulation data

All signals were analyzed with a custom-built Matlab program. For the verification of stimulus-locked responses, we fitted cortical EEGs to a Rayleigh distribution $V(s) = V_m s e^{\frac{1-s^2}{2}} \left(s = \frac{t}{\tau}\right)$ (Supplementary Method), where V_m and τ are the intensity and latency of the response, respectively, and t is the time. Fitting was applied to the early period (0–15 ms after stimulus onset) in which BF LFP was optogenetically evoked, and intermediate period (15–30 ms after stimulus onset) in which a prominent unimodal peak was observed in cortical EEGs (see Fig. 1e). EEGs were first de-trended and subtracted by the initial values to meet the boundary condition of the Rayleigh distribution.

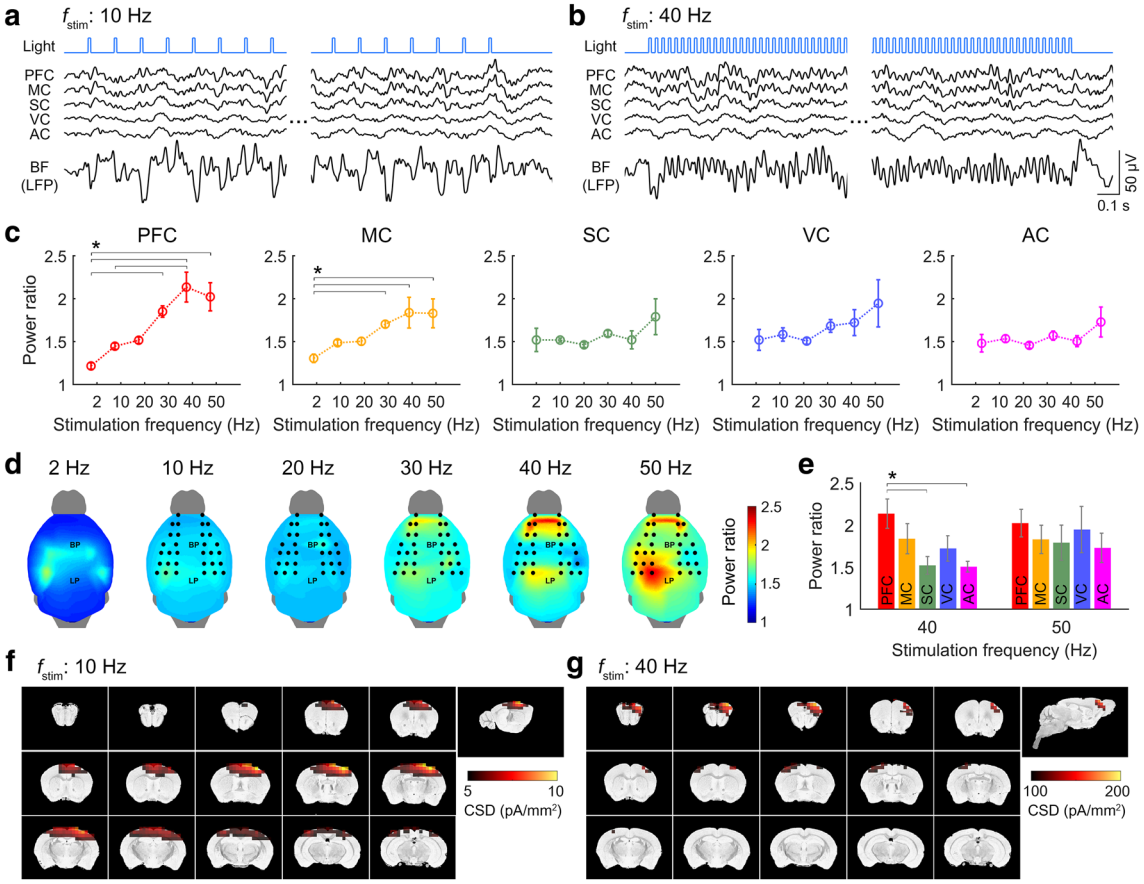

Fig. 2 Rhythmic stimulation of BF PV neurons at ~40 Hz preferentially enhances frontal cortex gamma band oscillations (GBO). **a, b** Representative EEG traces during optogenetic stimulation of BF PV neurons at 10 Hz and 40 Hz stimulation, respectively. *PFC* prefrontal, *MC* motor, *SC* somatosensory, *VC* visual, *AC* auditory, *BF* basal forebrain. To allow high time resolution, only the beginning (left) and end (right) of the 5-s stimulus train are shown. **c** Ratio of power during stimulation to baseline power at the stimulation frequency. PFC shows a resonance peak of power at 40 Hz whereas the other cortical areas did not show any frequency-specific response. In PFC and MC, stimulation at different frequencies resulted in significantly different evoked power (Friedman's ANOVA, $p < 0.05$) while the other regions did not. A post hoc analysis showed that 40 Hz stimulation resulted in significantly different response ($^*p < 0.05$, multiple comparison with Tukey–Kramer method) compared to low-frequency (2 and 10 Hz) stimulations in PFC. Error bars indicate SEM. See also Figure S1 for inter-trial coherence and phase-locking value. **d** Cortical topography of evoked power (fold ratio to pre-stimulus baseline) for various stimulation frequencies (2, 10, 20, 30, 40 and 50 Hz; stimulation pulse duration, 10 ms). PFC showed the largest increase of power in response to 40 Hz stimulation. Except for 2 Hz stimulation, all channels (marked with black dots) showed significantly increased power compared to pre-stimulus baseline (Wilcoxson signed rank test, $p < 0.05$) in response to optogenetic stimulation. **e** Evoked power in response to 40 Hz and 50 Hz stimulation. Evoked power was significantly large in PFC compared to posterior part of the brain regions such as SC and AC ($^*p < 0.05$, Friedman ANOVA and multiple comparison with Tukey–Kramer method). **f, g** Distributions of current source density (CSD) estimated by a minimum-norm current estimate algorithm. Note the strong focal activity at 40 Hz compared to broadly distributed activity at 10 Hz. The magnitude of the dipole strength was stronger for 40 Hz stimulation compared to 10 Hz by an order of magnitude (note different CSD scales in **f** and **g**)

Goodness-of-fit was evaluated by χ^2 test and the trials with $p < 0.05$ were determined to be well fitted. Distribution of the response intensities obtained from individual trials was tested with Wilcoxon rank-sum test, to determine whether the well-fitted response was significantly different from the baseline fluctuation (Fig. 1f).

Power, phase-locking value (PLV) and probability of significantly evoked activity (PSEA)

Fold change of power upon auditory stimulation (Fig. 2c–e) was calculated for each stimulation trial as $P = \frac{P_{\text{Stim}}}{P_{\text{Base}}}$, where P_{Stim} and P_{Base} are the power of $f_{\text{Stim}} \pm 2$ Hz band during the stimulation period and pre-stimulation baseline period, respectively. Power was calculated by fast Fourier transformation, and the initial 0.2-s period after sound onset was excluded from the calculation to remove the effect of event-related potentials on ongoing oscillation power. In the case of sole optogenetic stimulation, no onset-evoked potential was observed (Fig. S3a). PLV (Figs. S1b and S2c) was calculated as $\text{PLV} = \frac{1}{N}\left|\sum e^{-i\Delta\phi_x(t_k)}\right|$, where $\Delta\phi_x(t_k)$ is the phase difference between EEG signal x and stimulation pulse at time t_k, and N is the number of samples in the analysis period. Instantaneous phases of EEG were obtained by Hilbert transform of the band-pass ($f_{\text{Stim}} \pm 2$ Hz)-filtered EEG signals. A probability of observing significantly evoked activity (PSEA) was obtained by counting the number of trials with significantly evoked activity among all the trials. Deviant detection algorithm determines whether each trial has significantly evoked activity by comparing PLV to stimulation with confidence intervals of PLVs from surrogate data.

Topographic mapping

Topographic mapping is a procedure of 2-D interpolation of sparse data (34 channels of high-density EEG) onto the mouse brain surface (Figs. 1f, 2d, 3b). The mouse brain surface was rendered by *spm_surf*() function in SPM8 using the mouse magnetic resonance microscopy atlas (downloadable at http://www.loni.ucla.edu/). The colored surface was estimated with 2-D cubic spline interpolation based on the coordinates of the microarray.

Sound-evoked response latency

The sound-evoked response was defined as a trough point of 35–45 Hz band-pass-filtered EEG which followed the sound stimulation pulse. For each trial, the latency of the response was calculated with respect to the rising edge of the square-wave sound stimuli. The initial 0.2-s period was excluded from constructing response latency distribution.

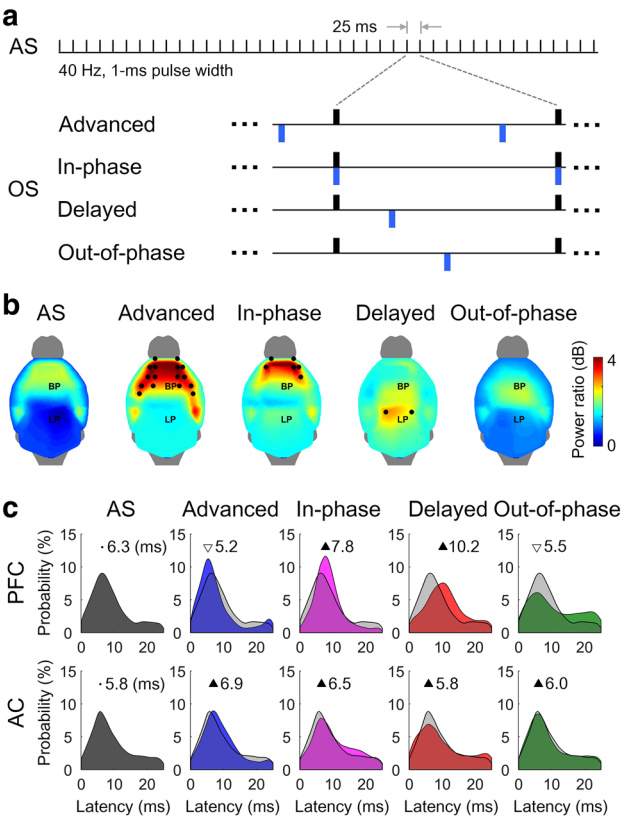

Fig. 3 Rhythmic 40 Hz stimulation of BF PV neurons in advance or in phase with 40 Hz auditory stimuli enhances gamma band responses in frontal–prefrontal and auditory cortices. **a** Experimental paradigm to test whether optogenetic stimulation of BF PV neurons affects the response to auditory stimulation (AS). Optical stimulation (OS) was administered at four different phases with respect to AS. *Advanced*: OS given 6.25 ms before AS, *in-phase*: OS given simultaneous with AS, *delayed*: OS given 6.25 ms after AS, and *out-of-phase*: OS given at the middle of two consecutive AS stimuli. The time interval between two consecutive AS is 25 ms (the period for 40 Hz). The order of OS conditions was randomly shuffled. AS and OS lasted 1 ms. **b** Cortical topography of evoked power (power ratio to pre-stimulus baseline) during ASSR and optogenetic BF stimulation delivered under conditions of different relative timing. The power ratio was presented in dB unit for contrast ($P = 10\log_{10}\frac{P_{\text{Stim}}}{P_{\text{Base}}}$). In each condition, the channels with significantly (Wilcoxson signed rank test, $p < 0.05$) increased power compared to AS alone were marked with black dots. Depending on the timing of BF PV activation, the auditory steady-state response (ASSR) dramatically increased (during *advanced* and *in-phase* interventions). See also Figure S2 for averaged EEG traces, power and phase-locking value with different interventions. **c** Response latency distributions, relative to each sound click, in prefrontal cortex (upper, PFC) and auditory (lower, AC) cortex show sharp synchronization in *in-phase* and *advanced* BF stimulations. The control distribution of AS alone is overlaid with gray color onto the distribution obtained for each timing condition. Triangles and numbers above each trace indicate the latency with maximal probability, in ms. Advanced and delayed phase responses compared to AS were marked as white and black triangles, respectively. Note that *advanced* and *in-phase* BF PV stimulation lead to sharpened distributions of response latencies in PFC preceding (5.2 ms) or following (7.8 ms) AS, and in AC where response latencies followed AS (6.5–6.6 ms)

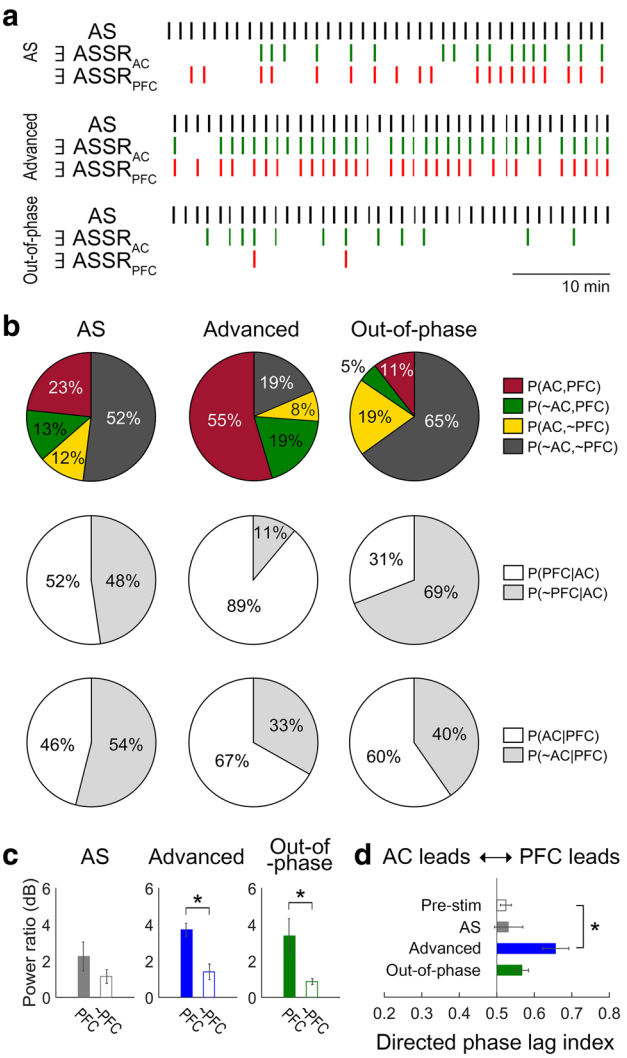

Fig. 4 Stimulation of BF PV neurons in advance to auditory stimuli increases the probability of auditory steady-state responses (ASSR) in prefrontal cortex (PFC) and auditory cortex (AC) and enhances top-down control of AC by PFC. **a** Raster plots showing the presence of significant ASSR in auditory (AC, green bars) and frontal-prefrontal (PFC, red bars) cortex during auditory steady-state stimulation (black bars). Significance of the ASSR for individual trials was determined by deviant detection algorithm when the auditory stimulation (AS) was given without intervention (upper row, AS), when the BF PV stimulation was given in advance of AS by 6.25 ms (middle row, *advanced*), and when the BF PV stimulation was given in an anti-phasic manner to AS (lower row, *out-of-phase*). These raster plots show the non-stationary nature of ASSR; not every sound evoked significant ASSR. **b** Stimulation timing strongly affects the likelihood of conjoint responses in PFC and AC. Individual trials were analyzed to determine if they elicited a significant response. Responses in individual trials were considered significant if the power at gamma band frequencies exceeded a 95% confidence interval of the baseline gamma power. See also Fig. S4 for all the intervention conditions. 1st row: the pie charts illustrate the probability of a significant response in both PFC and AC, *P*(AC, PFC), in PFC alone, *P*(~AC, PFC), in AC alone, P(AC, ~PFC) or in neither region, P(~AC, ~PFC). 2nd row: conditional probability of a significant ASSR response in PFC given a significant ASSR in AC, $P(\mathrm{PFC} \mid \mathrm{AC})$. 3rd row: conditional probability of ASSR in AC given ASSR in PFC, $P(\mathrm{AC} \mid \mathrm{PFC})$. The *advanced* stimulation increased the consistency of ASSR by increasing conjoint activity of ASSR in both AC and PFC whereas *out-of-phase* stimulation caused the reverse effect. **c** Significant ASSR in PFC increases ASSR power in the auditory cortex. The diagrams show ASSR power ratio in auditory cortex in the presence (PFC) and absence (~PFC) of significant PFC response. The difference was significant for *advanced* and *out-of-phase* conditions ($^*p < 0.05$, Wilcoxon rank-sum test). **d** In the *advanced* stimulation condition phase relationship analysis indicates enhanced PFC driving of the response in AC. The phase relationship between ASSR in PFC and AC were investigated by calculating directed phase lagging index, ranging from 0 (AC drives PFC) to 1 (PFC drives AC). *Significant difference. Wilcoxon signed rank test was performed for comparison of pre-stimulus versus stimulus periods. Friedman's ANOVA and post hoc comparison with Tukey–Kramer method was applied for the group comparisons between stimulation conditions

From the pool of response latency, probability mass function was estimated by kernel smoothing density estimate using the normal distribution (Fig. 3c).

Directed phase lag index (dPLI), phase synchronization index (PSI), and connectogram

dPLI (Fig. 4d) was calculated as $\mathrm{dPLI} = \frac{1}{N}\sum H\left(\Delta\phi_{xy}(t_k)\right)$, where $H(\cdots)$ is a Heaviside step function, $\Delta\phi_{xy}(t_k)$ is the phase difference between two signals x and y at time t_k, and N is the number of samples in the analysis period. PSI (Fig. 5a–c) between signals was calculated as $\mathrm{PSI} = \frac{1}{N}\left|\sum \mathrm{e}^{-i\Delta\phi_{xy}(t_k)}\right|$. Instantaneous phases were obtained by Hilbert transform of the band-pass ($f_{\mathrm{Stim}} \pm 2$ Hz)-filtered EEG signals. The circular connectogram (Fig. 5c) depicts the channel pairs with robust connection during stimulation. For each trial, the significance of PSI increase during the stimulation was first determined by deviant detection algorithm. Robustness of the connection was determined by the proportion of trials which showed a significant increase of PSI during the stimulation, and the channel pairs with the proportion higher than 50% were connected with yellow lines.

Statistical analysis

The intra-animal variance in our data was more significant than inter-animal variance. Hence, after checking the statistical independence on the individual animals, we used all trials from all animals as the ensemble data set for analysis. Statistical significance of fold power change in response to stimulation at different frequencies was tested with repeated measures ANOVA (Friedman's test) and post hoc comparisons were performed by Tukey–Kramer method (Fig. 2c, e). PLV during stimulation was compared to surrogate dataset constructed by phase randomization with rank-sum test (Fig. S1b). Evoked power of ASSR for

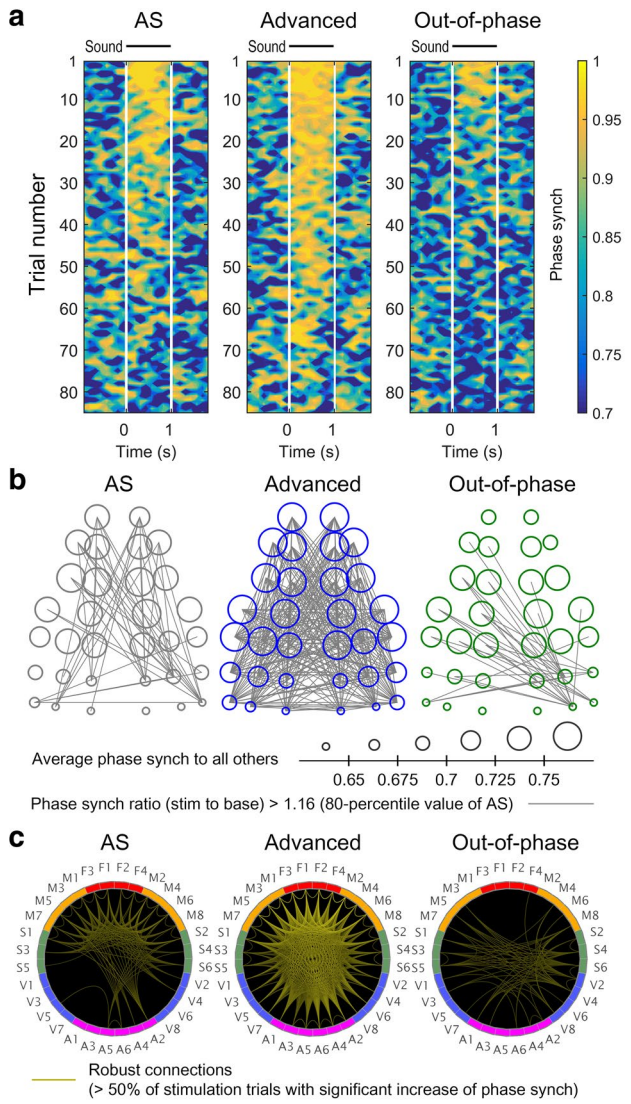

Fig. 5 BF PV stimulation in advance to auditory stimuli reorganizes the cortical network in favor of stronger long-range interactions between prefrontal cortex (PFC) and auditory cortex (AC). **a** Phase synchrony between PFC and AC for individual trials in different stimulation conditions. Trials were sorted in descending order of the average phase synchrony during the auditory stimulation (from time 0–1 s). **b** Changes in cortical ASSR networks during BF PV stimulation according to phase synchrony between different channels under the different stimulation conditions. Node size indicates the strength of phase synchrony averaged over all the pairs connecting with all other leads. Lines represent the connections which showed significantly enhanced phase synchrony (threshold: 80 percentile value of AS phase synchrony ratio). *Advanced* stimulation increased phase synchrony throughout the network with the maximal enhancement in PFC, whereas *out-of-phase* stimulation largely diminishing phase synchrony throughout the network. **c** Connectograms illustrating the robustness of the ASSR network. The robust connection between two channels (yellow lines) was defined established when the phase synchrony between the channels was found significantly increased in more than 50% of the individual trials during stimulation. The significance of phase synchrony was determined by deviant detection algorithm

each optogenetic intervention condition was compared to naïve ASSR power by signed rank test (Fig. 3b). The difference in ASSR response latency distribution was tested with two-sample Kolmogorov–Smirnov test (Fig. 3c). Evoked power of ASSR and PLV under optogenetic intervention conditions were tested with repeated measures ANOVA (Friedman's test) and post hoc comparisons were performed by Tukey–Kramer method (Fig. S3b, c). ASSR power in auditory cortex with or without frontal ASSR power was tested with rank-sum test (Fig. 4c). dPLI during ASSR with optogenetic intervention were tested with repeated measures ANOVA (Friedman's test) and post hoc comparisons were performed by Tukey–Kramer method (Fig. 4d). For all tests, we used $p = 0.05$ as the significance threshold.

Results

Cortical responses to single-pulse optical stimulation of BF PV neurons

To determine the effect of stimulation of BF PV neurons on the spatio-temporal patterns of cortical electrical activity, we combined unilateral BF PV-specific optogenetic stimulation with hdEEG recordings in the mouse (opto-hdEEG, Fig. 1a). We targeted the magnocellular preoptic (MCPO) area for optical stimulation since this subregion of the BF contains a high density of PV neurons (McKenna et al. 2013). Immunohistochemical staining confirmed correct targeting and selective transduction of BF PV neurons (Fig. 1b), as in our previous study (Kim et al. 2015). Our custom-designed mouse hdEEG arrays were used to record the topography of the cortical responses (Fig. 1c).

We first characterized the cortical responses to *single-pulse* stimulation of BF PV neurons (optical pulse duration = 10 ms, 6360 trials). Single-pulse stimulation of BF PV neurons generated significant activity in many cortical regions when compared to baseline fluctuation (Fig. 1d). The cortical regions affected by BF PV neurons were determined by comparing the fit of the early (P1, 0–15 ms) and intermediate (N1, 15–30 ms) parts of the evoked cortical potentials (Fig. 1e) to a Rayleigh function (χ^2 goodness-of-fit, $p < 0.05$, Supplementary Methods). Briefly, the trials with LFPs which fit a Rayleigh function were sorted out and classified as a significantly activated trial if the peaks exceed the confidence interval of baseline fluctuations. The prefrontal, motor, and auditory cortices presented a significant P1 peak and the prefrontal cortices demonstrated a significant N1 peak compared to baseline fluctuations (Wilcoxon rank-sum test, $p < 0.05$). The ratios of significantly activated trials to total trials were $5.9 \pm 0.7\%$ and $6.0 \pm 1.2\%$ for P1 and N1 peaks,

respectively. The average P1 peak amplitudes were 5.4, 4.9, 4.7, 0.5, and 1.3 μV for prefrontal, motor, somatosensory, visual and auditory cortices, respectively. The average N1 peak amplitudes were −5.1, −3.2, 1.9, 3.6, and 1.5 μV for prefrontal, motor, somatosensory, visual and auditory cortices, respectively. The latency was similar across the regions with mean latency of 6.3 ± 0.004 ms and 21.3 ± 0.002 ms for P1 and N1 peaks, respectively. The topography of P1 and N1 responses are depicted in Fig. 1f.

Rhythmic activation of BF PV neurons at 40 Hz preferentially enhanced prefrontal cortex gamma oscillations

Although the response to single-pulse stimulation confirmed significant effects of BF PV neuron stimulation on cortical activity, BF PV neurons normally discharge at high frequencies during active brain states (Xu et al. 2015; Duque et al. 2000). Thus, to investigate the frequency dependence of the effect of BF PV neurons on the topography of cortical rhythms, we selectively and repetitively stimulated BF PV neurons at various stimulation frequencies (f_{Stim}=2, 10, 20, 30, 40, and 50 Hz; pulse duration = 10 ms; stimulation duration = 5 s; inter-stimulus interval = 10 s) in a randomly shuffled order, and recorded the hdEEG response. In each mouse, this optical stimulation was repeated 60 times per f_{Stim}. Figure 2a, b shows the EEG responses in five different cortical areas and the LFP in the BF averaged over trials for a representative mouse. In the BF LFP, a negative peak time-locked to the optical pulse was visible in time traces for both 10 and 40 Hz, indicating synchronous activation of BF PV neurons. BF PV neurons are connected by gap junctions (McKenna et al. 2013), so this simultaneous optogenetic stimulation likely mimics their naturally synchronous discharge, consistent with observations of gamma band fluctuations in local field potential recordings in BF during spontaneous wakefulness (Nair et al. 2016).

In the cortex, stimulus-locked responses were not prominent in the raw traces for stimulation at 2, 10 or 20 Hz, but stimulus-locked oscillations were pronounced for 40 Hz and 50 Hz stimulation (Fig. 2a, b), particularly over frontal cortex. Next, we examined the effects of *individual animals* and *stimulation frequency* in each region using multiple comparison tests. We found there were no significant difference in the responses between individual mice ($p > 0.05$, Friedman ANOVA) but there was a significant effect from stimulation frequency in prefrontal and motor cortex ($p = 0.0004$, $dF = 5$, $\chi^2 = 28.1$ for prefrontal and $p = 0.003$, $dF = 5$, $\chi^2 = 17.9$ for motor cortex, Friedman ANOVA, Table S2).

We plotted the evoked power ratio in different cortical regions with respect to the stimulation frequency (Fig. 2c). PFC showed a resonant frequency of 40 Hz, in good agreement with previous findings (Kim et al. 2015). For other cortical regions (e.g., SC, VC, and AC), increased power was observed at the stimulation frequency but with no apparent resonance peak ($p < 0.05$, Friedman's ANOVA and post hoc comparisons with Tukey–Kramer method).

The cortical topographies of the change of power induced at various stimulation frequencies are shown in Fig. 2d (hdEEG signals were filtered at cutoff frequencies = f_{Stim} ± 2 Hz, normalized by pre-stimulus power and ensemble-averaged). Compared to the baseline, the power increased in most of the regions as marked by black dots (Wilcoxson signed rank test, $p < 0.05$). As stimulation frequency varies, the topographical responses changed in a way that a prominent response occurs in the prefrontal cortex at gamma band (Fig. 2e).

We further visualized the influence of stimulation by estimating the equivalent dipole source for the grand-averages of evoked power. We used the minimum-norm estimate algorithm and boundary element model (Lee et al. 2013a). Figure 2f, g shows that the reconstructed source distributions are compatible with the topographies in Fig. 2d. Stimulation at 40 Hz shows a more focal activation of the PFC (anterior cingulate, secondary motor and orbitofrontal regions) compared to the dispersed distribution reconstructed for 10 Hz. The magnitude of the dipole strength was stronger for 40 Hz stimulation compared to 10 Hz by an order of magnitude.

To investigate the reliability of the evoked power with respect to the stimulation, we examined the time courses of the inter-trial coherence (ITC) to measure consistency in timing response to BF PV stimulation (Fig. S1a). The ITC plots showed that 40 Hz stimulation of BF PV neurons generated a consistent response in PFC in terms of phase dynamics. We found a significant main effect in the whole-time block particularly at 40 Hz stimulation and the evoked response was the largest for PFC. The increased phase-locking value and reliability of evoked oscillations are presented in Fig. S1b, c, respectively, and time traces of evoked EEG for each brain region with different stimulation frequency are presented in Fig. S2.

Rhythmic phase-locked stimulation of BF PV neurons tunes auditory steady-state responses (ASSR)

Since BF PV stimulation most strongly affected GBO in frontal cortex and previous studies have shown an influence of frontal cortex on GBO in primary sensory cortices (Gregoriou et al. 2009), we next asked whether stimulation of BF PV neurons would enhance cortical GBO induced by 1-s trains of 40 Hz auditory stimuli (auditory steady-state response, ASSR; 85 dB; pulse duration = 1 ms, stimulation duration = 1 s; inter-stimulus interval = 2 s;

200 repetitions), and if so, determine the optimal phase relationship between optical stimulation of BF PV neurons and delivery of auditory stimuli. BF PV neurons were stimulated during ongoing auditory steady-state stimulation with a low light power to prevent any overwhelming responses to optical stimulation (1.2 mW; pulse duration = 1 ms) at various phase differences between the onset of sound and optical stimulation. The experiment was performed in a beaker to maintain the constant level of sound pressure, and during the experiment, the mice stayed awake for most of the time maybe due to the loud sound. Variant behavioral states were observed including grooming, sniffing, actively moving, etc. As depicted in Fig. 3a, we tested four distinct phase differences between sound and optical stimulation which we refer to as *advanced* (optical stimulation of BF PV neurons 6.25 ms before tone, i.e. one quarter of the cycle), *in-phase* (0 ms difference), *delayed* (6.25 ms after the tone), and *out-of-phase* (12.5 ms before/after tone, i.e., half a cycle) interventions. The influences of rhythmic stimulation of BF PV neurons were compared to auditory stimulation (AS) alone.

The cortical topographies of ASSR power were plotted under the different conditions of BF PV stimulation (Fig. 3b). Strikingly different results were apparent for *advanced* and *in-phase* stimulation versus *out-of-phase* and *delayed* stimulation. *Advanced* and *in-phase* stimulations magnified the ASSR response in frontal cortex compared to auditory stimulation (AS) alone (Wilcoxon signed rank test, $p < 0.05$). On the other hand, *delayed* and *out-of-phase* stimulations did not significantly alter ASSR power. The time traces of ASSR in different conditions are presented in Fig. S3a and the power and phase-locking values are presented in Fig. S3b–c.

To determine how stimulation of BF PV neurons affected the temporal distribution of responses to the ASSR, we detected the peaks of individual evoked potentials with respect to individual sound pulses from all trials and all mice and then the peak latencies were collected to plot the latency distribution (Fig. 3c). The maximum probability, the most probable latency, and the response range were calculated and summarized in Table 1. The frontal cortex was activated more promptly in the *advanced* stimulation condition compared to other conditions, whereas the peak response in auditory cortex was delayed.

Advanced stimulation of BF PV neurons increases the influence of frontal cortex on auditory cortex

Previous studies have shown that activation of prefrontal cortex can influence the generation of GBO in sensory cortices (Gregoriou et al. 2009; Schadow et al. 2009). To examine whether stimulation of BF PV neurons would affect the likelihood of conjoint GBO responses in prefrontal cortex and auditory cortex, we analyzed responses in individual trials under the different conditions. As depicted in the representative time trace of ASSR occurrence in Fig. 4a, ASSR occurred irregularly. The probability of events was calculated from each mouse and ensemble-averaged. We found that in unperturbed condition, the co-occurrence rate of ASSR in PFC and AC was 23% whereas the no-response rate was 52% (left panels in Fig. 4b). The probability of events changed dramatically by BF PV intervention: during *advanced* stimulation, the co-occurrence rate increased to 55% from 23% and the no-response rate dropped to 19% (middle panels in Fig. 4b). Oppositely, during *out-of-phase* stimulation, the no-response rate increased to 65% and the co-occurrence rate dropped to 11%. The high input/

Table 1 Summary of the distribution parameters of response latency

	Parameters	AS	Advanced	In-phase	Delayed	Out-of-phase	Continuous
PFC	P_{max}	0.09	0.11	0.12	0.08	0.06	0.09
	τ_{max} (ms)	6.3	5.2	7.8	10.2	5.5	6.4
	FWHM (ms)	9.1	7.2	7.0	10.8	11.5	8.5
	$[\tau_1, \tau_2]$ (ms)	[2.1, 11.2]	[1.8, 9.0]	[4.2, 11.2]	[4.3, 15.1]	[0.7, 12.2]	[2.4, 10.9]
AC	P_{max}	0.09	0.09	0.08	0.07	0.09	0.09
	τ_{max} (ms)	5.8	6.9	6.5	5.8	6.0	6.0
	FWHM (ms)	8.6	9.5	9.2	11.3	8.5	7.8
	$[\tau_1, \tau_2]$ (ms)	[2.2, 10.9]	[2.9, 12.4]	[3.0, 12.2]	[0.7, 12.0]	[1.7, 10.2]	[2.4, 10.3]

P_{max} is the maximum probability and τ_{max} is the latency at P_{max}. Full width at half maximum (FWHM) is the difference of two cutoff values of latency at which the probability is half of P_{max}. The dynamic range for most likely observed latency values, $[\tau_1,\tau_2]$, are the two extreme values for FWHM. FWHM measures the sharpness of the distribution and is often used to assess the temporal precision of the system. In naïve AS, FWHM in AC was shorter than in PFC, meaning that AC react to the sound stimuli in a more temporally precise way compared to PFC. This pattern was switched, however, under the advanced stimulation: FWHM in PFC was shorter than in AC, indicating that advanced stimulation made PFC more agile to sound pulse. On the other hand, under the out-of-phase stimulation, the dynamic range for the response in PFC became wider, meaning the responses at PFC became unpredictable

Table 2 Co-occurrence and conditional occurrence rate of ASSR in PFC and AC

	AS	Advanced	In-phase	Delayed	Out-of-phase	Continuous
P(PFC)	0.36	**0.74**	0.52	0.27	**0.16**	0.34
P(AC)	0.35	**0.64**	0.46	0.35	**0.30**	0.37
P(AC, PFC)	0.23	**0.55**	0.36	0.18	**0.11**	0.25
P(AC, ~PFC)	0.12	**0.08**	0.10	0.17	**0.19**	0.12
P(~AC, PFC)	0.13	**0.19**	0.16	0.09	**0.05**	0.09
P(~AC, ~PFC)	0.52	**0.19**	0.38	0.56	**0.65**	0.54
P(PFC|AC)	0.52	**0.89**	0.70	0.45	**0.31**	0.66
P(AC|PFC)	**0.46**	**0.67**	0.54	0.56	0.60	0.57

The highest probability to have the most ASSR was observed when BF PV was activated in advance to the sound: 74% of sound evoked ASSR in PFC and only 19% of sound did not evoke ASSR. On the hand, when the BF PV was activated alternatively to the sound rhythm (i.e., out-of-phase), PFC was almost inert to the sound input. Most importantly, P(PFC) ranged between 0.16 and 0.74 depending on the intervention condition, indicating that PFC is strongly modulated by BF PV intervention. Bold font is used to indicate the highest and lowest probabilities under the different conditions

output feature shown in *advanced* stimulation was similar in *in-phase* stimulation and the inactivity shown in *out-of-phase* stimulation was similar in *delayed* stimulation with a smaller magnitude of the effect (Fig. S3 and Table 2). Furthermore, the power of the ASSR in auditory cortex was enhanced when there was a significant response in frontal cortex (Fig. 4c). Phase relationship analysis showed that the information flow from PFC to AC increased in a significant way during *advanced* stimulation (Fig. 4d). Together, these results suggest that *advanced* BF PV stimulation enhances the influence of frontal cortex on auditory cortex GBO.

BF PV reorganizes the cortical network of auditory steady-state responses: advanced or in-phase stimulation promotes formation of a *global workspace*

Stimulation of BF PV neurons in advance of auditory stimuli boosted the cortical responses, reminiscent of the effect of increased arousal (Linden et al. 1985; Plourde 1996) and attention on the ASSR (Tiitinen et al. 1993). Although speculative, our findings suggest that BF PV neurons might facilitate global integration of sensory information and facilitate the formation of a global workspace for conscious perception involving increased interactions within cortical hubs and increased long-range synchronization of neuronal activity at gamma band frequencies (Dehaene and Changeux 2011; Kitzbichler et al. 2011). Thus, next we investigated how stimulation of BF PV neurons changes the cortical network configuration.

Examination of the functional connectivity of cortical ASSR networks according to the consistency of phase synchrony between different nodes of the network under the different stimulation conditions confirmed our predictions of increased long-range synchronization and increased interaction between cortical hubs. Advanced stimulation increased long-range phase synchrony between PFC and auditory cortices, compared to AS or *out-of-phase* stimulation (Fig. 5a). *Advanced* stimulation affected the whole cortical network of GBO so that the changes in network topology were associated with the emergence of long-distance synchrony (Fig. 5b). At each node, the average of phase synchrony with other nodes was indicated by node size. *Advanced* stimulation increased the diameter of nodes whereas *out-of-phase* stimulation reduced it. Investigation of the percentage of trials which significantly increased phase synchrony compared to baseline values (Fig. 5c), revealed that *advanced* stimulation increased the robustness of communication between frontal and sensory cortices, whereas *out-of-phase* stimulation essentially disconnected the cortical ASSR network.

Discussion

How subcortical arousal systems modulate the spatio-temporal dynamics of cortical electrical activity is an important unresolved question with translational implications. Thus, here for the first time, we combined selective optogenetic stimulation of a defined subcortical neuronal cell-type, BF PV neurons, with high-density EEG recordings in mice (opto-hdEEG) and examined the effect on an auditory stimulation paradigm used to detect cortical processing abnormalities in neuropsychiatric disorders. We found that rhythmic stimulation of BF PV neurons at frequencies within their normal physiological firing range (Kim et al. 2015; Xu et al. 2015), exerted a potentiation of GBO in auditory cortex and reorganized the cortical topography of responses in a manner consistent with increased attention or awareness.

A handful of previous studies have examined the effect of stimulation of particular subcortical arousal systems on whole-brain activity, by combining optogenetic stimulation with positron emission tomography (opto-PET) (Thanos

et al. 2013) or functional magnetic resonance imaging (opto-fMRI) (Lee et al. 2017). Our hdEEG arrays have the additional advantage of millisecond temporal resolution and allow comparison with human hdEEG studies. Thus, opto-hdEEG is an important technique for understanding the effect of subcortical arousal systems on the spatio-temporal patterns of cortical electric activity.

We focused our study on the BF, an important component of the ascending reticular activating system involved in cortical activation, attention and reward processing (Yang et al. 2017). Previous electrical stimulation, lesion and pharmacological stimulation studies have shown that BF promotes cortical GBO (Brown et al. 2012). Furthermore, coherence and Granger causality analysis of local field potential recordings from BF and visual cortex suggested that BF drives gamma oscillations in visual cortex (Nair et al. 2016). A previous optogenetic study from our group indicated that cortically projecting GABAergic neurons containing PV appear to have a special role in modulating cortical GBO, in part through their targeting of cortical PV interneurons (Kim et al. 2015). However, it was unclear how BF PV neurons affect the spatio-temporal dynamics of cortical electrical activity. Our results using opto-hdEEG show that stimulation of BF PV neurons at gamma band frequencies, mimicking their discharge during wakefulness and REM sleep (Kim et al. 2015; Xu et al. 2015) elicited the most pronounced, reliable and consistent responses, with a focus in the frontal cortex whereas single-pulse or low-frequency stimulation had widespread effects on cortical activity which included many frequency bands. This strongly indicates that dynamic modulation of cortical activity cannot be simply predicted from the cortical projection patterns of arousal systems, and necessitate studies using opto-hdEEG or similar methodology.

In addition to the topography of basal forebrain projections to the cortex (Zaborszky et al. 2013), the dynamic pattern of cortical responses depends on the resonant properties of individual cortical regions as well as cortico–cortical and cortical–subcortical interactions. Our previous study (Kim et al. 2015) showed that optogenetic BF PV stimulation entrains a resonant 40 Hz oscillator within frontal cortex. Previous studies in humans (Rosanova et al. 2009) have shown that frontal corticothalamic circuits are more primed to generate a resonance response at gamma frequencies than other cortical areas, which may partly explain the predominance of frontal GBO responses in our study. Although direct projections of BF GABA/PV neurons to cortical interneurons in frontal cortex are the most parsimonious explanation of this response, other projections of BF GABA/PV neurons, for instance to the thalamic reticular nucleus (Kim et al. 2015), may also play a role. Future studies should tease out the role of these different pathways.

BF GABAergic neurons play an important role in attention (Burk and Sarter 2001), as do the cortical PV neurons to which they project (Kim et al. 2016). One well-known effect of attention is an enhancement of sensory stimuli-evoked GBO (Tiitinen et al. 1993; Skosnik et al. 2007), mediated by an influence of the frontal cortex on primary sensory cortices (Gregoriou et al. 2009). Our hdEEG study examined whether concomitant rhythmic stimulation of BF PV could enhance the ASSR in a manner similar to the effects of attention. Analysis of the phase relationship revealed that BF PV stimulation most profoundly enhanced auditory stimuli-driven GBO when stimulated in advance of sound onset. Several features of the cortical responses to *advanced* BF PV stimulation were consistent with the effects of attention. *Advanced* BF PV stimulation enhanced frontal cortex control of GBO in the auditory cortex and reorganized the cortical network such that long-range interactions at gamma band frequencies were facilitated. In addition, stimulation of BF PV neurons tuned the amplitude of ASSR in both auditory and prefrontal cortex and sharpened the temporal profiles.

Human and non-human primate studies have shown that attention, working memory and conscious awareness of sensory stimuli are associated with a profound reorganization of cortical activity patterns (Dehaene and Changeux 2011; Kitzbichler et al. 2011; Gross et al. 2004). According to the *global workspace* model these higher-level cognitive processes lead to *ignition* of a cortical network, allowing broadcasting of information between functionally related nodes of the cortical network. The activity of integrative hubs is enhanced and long-range cortical activity within the beta and gamma bands of the EEG is facilitated (Dehaene and Changeux 2011). Our results suggest that increased rhythmic activity of BF PV neurons may play a role in such a reorganization of cortical activity. Synchronization of frontal cortex hubs and long-range cortical interactions within the gamma band were enhanced, as in human studies of working memory (Kitzbichler et al. 2011) or conscious awareness (Dehaene and Changeux 2011). Many severe neuropsychiatric conditions such as vegetative state, schizophrenia and Alzheimer's disease are associated with deficits in attention, working memory and awareness, associated with impaired frontal control and generation of GBO. Our results suggest that therapies which enhance the synchronous, rhythmic discharge of BF PV neurons at gamma band frequencies may be effective in mitigating these deficits.

Acknowledgements This work was performed at Korea Institute of Science and Technology and was supported in part by U.S. Veterans Administration, US National Institutes of Health Grant RO1 MH039683, the National Research Council of Science and technology of Korea (CRC-15-04-KIST) and the National Research Foundation of Korea (2017R1A2B3012659). REB and JTM received partial salary support from United States VA Biomedical Laboratory Research and

Development Service Award I01BX001356. JMM is supported by VA CDA IK2BX002130. Additional salary support was provided by US National Institutes of Health Grants R01 MH100820, R21 NS079866 and R21 NS093000. REB, JTM and JMM are Research Health Scientists at VA Boston Healthcare System. The contents of this work do not represent the views of the U.S. Department of Veterans Affairs or the United States Government. This work also reflects the intellectual contribution and mentorship of Prof. Robert W. McCarley, who sadly passed away during the final stages of this project.

Compliance with ethical standards

Conflict of interest The authors report no competing financial interests. JTM also received partial salary compensation and funding from Merck MISP (Merck Investigator Sponsored Programs) but has no conflict of interest with this work.

References

Berger H (1929) Ueber das elektroenkephalogramm des Menschen. Arch Psychiatr Nervenkr 87:527–570

Brown RE, Basheer R, McKenna JT, Strecker RE, McCarley RW (2012) Control of sleep and wakefulness. Physiol Rev 92(3):1087–1187

Burk JA, Sarter M (2001) Dissociation between the attentional functions mediated via basal forebrain cholinergic and GABAergic neurons. Neuroscience 105(4):899–909

Cardin JA, Carlen M, Meletis K, Knoblich U, Zhang F, Deisseroth K, Tsai LH, Moore CI (2009) Driving fast-spiking cells induces gamma rhythm and controls sensory responses. Nature 459(7247):663–667

Cardin JA, Carlen M, Meletis K, Knoblich U, Zhang F, Deisseroth K, Tsai LH, Moore CI (2010) Targeted optogenetic stimulation and recording of neurons in vivo using cell-type-specific expression of Channelrhodopsin-2. Nat Protoc 5(2):247–254. https://doi.org/10.1038/nprot.2009.228

Carlen M, Meletis K, Siegle JH, Cardin JA, Futai K, Vierling-Claassen D, Ruhlmann C, Jones SR, Deisseroth K, Sheng M, Moore CI, Tsai LH (2012) A critical role for NMDA receptors in parvalbumin interneurons for gamma rhythm induction and behavior. Mol Psychiatry 17:537–548

Choi JH, Koch KP, Poppendieck W, Lee M, Shin HS (2010) High resolution electroencephalography in freely moving mice. J Neurophysiol 104(3):1825–1834

Crone NE, Boatman D, Gordon B, Hao L (2001) Induced electrocorticographic gamma activity during auditory perception. Brazier Award-winning article, 2001. Clin Neurophysiol Off J Int Fed Clin Neurophysiol 112(4):565–582

Dehaene S, Changeux JP (2011) Experimental and theoretical approaches to conscious processing. Neuron 70(2):200–227

Duque A, Balatoni B, Detari L, Zaborszky L (2000) EEG correlation of the discharge properties of identified neurons in the basal forebrain. J Neurophysiol 84(3):1627–1635

Franklin K, Paxinos G (2008) The mouse brain in stereotaxic coordinates, 3rd edn. Academic Press, North Ryde

Fries P (2009) Neuronal gamma-band synchronization as a fundamental process in cortical computation. Annu Rev Neurosci 32:209–224

Gray CM, Singer W (1989) Stimulus-specific neuronal oscillations in orientation columns of cat visual cortex. Proc Natl Acad Sci USA 86(5):1698–1702

Gregoriou GG, Gotts SJ, Zhou H, Desimone R (2009) High-frequency, long-range coupling between prefrontal and visual cortex during attention. Science 324(5931):1207–1210

Gross J, Schmitz F, Schnitzler I, Kessler K, Shapiro K, Hommel B, Schnitzler A (2004) Modulation of long-range neural synchrony reflects temporal limitations of visual attention in humans. Proc Natl Acad Sci USA 101(35):13050–13055. https://doi.org/10.1073/pnas.0404944101

Hong LE, Summerfelt A, McMahon R, Adami H, Francis G, Elliott A, Buchanan RW, Thaker GK (2004) Evoked gamma band synchronization and the liability for schizophrenia. Schizophr Res 70(2–3):293–302. https://doi.org/10.1016/j.schres.2003.12.011

Kim T, Thankachan S, McKenna JT, McNally JM, Yang C, Choi JH, Chen L, Kocsis B, Deisseroth K, Strecker RE, Basheer R, Brown RE, McCarley RW (2015) Cortically projecting basal forebrain parvalbumin neurons regulate cortical gamma band oscillations. Proc Natl Acad Sci USA 112(11):3535–3540

Kim H, Ahrlund-Richter S, Wang X, Deisseroth K, Carlen M (2016) Prefrontal parvalbumin neurons in control of attention. Cell 164(1–2):208–218. https://doi.org/10.1016/j.cell.2015.11.038

Kitzbichler MG, Henson RN, Smith ML, Nathan PJ, Bullmore ET (2011) Cognitive effort drives workspace configuration of human brain functional networks. J Neurosci 31(22):8259–8270. https://doi.org/10.1523/JNEUROSCI.0440-11.2011

Korotkova T, Fuchs EC, Ponomarenko A, von EJ, Monyer H (2010) NMDA receptor ablation on parvalbumin-positive interneurons impairs hippocampal synchrony, spatial representations, and working memory. Neuron 68(3):557–569

Kwon JS, O'Donnell BF, Wallenstein GV, Greene RW, Hirayasu Y, Nestor PG, Hasselmo ME, Potts GF, Shenton ME, McCarley RW (1999) Gamma frequency-range abnormalities to auditory stimulation in schizophrenia. Arch Gen Psychiatry 56(11):1001–1005

Lee M, Kim D, Shin HS, Sung HG, Choi JH (2011) High-density EEG recordings of the freely moving mice using polyimide-based microelectrode. J Vis Exp. https://doi.org/10.3791/2562

Lee C, Oostenveld R, Lee SH, Kim LH, Sung H, Choi JH (2013a) Cortical source localization of mouse extracranial electroencephalogram using the FieldTrip toolbox. Conf Proc IEEE Eng Med Biol Soc 2013:3307–3310. https://doi.org/10.1109/EMBC.2013.6610248

Lee C, Oostenveld R, Lee SH, Kim LH, Sung H, Choi JH (2013b) Dipole source localization of mouse electroencephalogram using the Fieldtrip toolbox. PLoS One 8(11):e79442. https://doi.org/10.1371/journal.pone.0079442

Lee JH, Kreitzer AC, Singer AC, Schiff ND (2017) Illuminating neural circuits: from molecules to MRI. J Neurosci 37(45):10817–10825. https://doi.org/10.1523/JNEUROSCI.2569-17.2017

Linden RD, Campbell KB, Hamel G, Picton TW (1985) Human auditory steady state evoked potentials during sleep. Ear Hear 6(3):167–174

McKenna JT, Yang C, Franciosi S, Winston S, Abarr KK, Rigby MS, Yanagawa Y, McCarley RW, Brown RE (2013) Distribution and intrinsic membrane properties of basal forebrain GABAergic and parvalbumin neurons in the mouse. J Comp Neurol 521:1225–1250

Munk MH, Roelfsema PR, Konig P, Engel AK, Singer W (1996) Role of reticular activation in the modulation of intracortical synchronization. Science 272(5259):271–274

Nair J, Klaassen AL, Poirot J, Vyssotski A, Rasch B, Rainer G (2016) Gamma band directional interactions between basal forebrain and visual cortex during wake and sleep states. J Physiol Paris 110(1–2):19–28. https://doi.org/10.1016/j.jphysparis.2016.11.011

O'Donnell BF, Vohs JL, Krishnan GP, Rass O, Hetrick WP, Morzorati SL (2013) The auditory steady-state response (ASSR): a translational biomarker for schizophrenia. Suppl Clin Neurophysiol 62:101–112

Plourde G (1996) The effects of propofol on the 40-Hz auditory steady-state response and on the electroencephalogram in humans. Anesth Analg 82(5):1015–1022

Rosanova M, Casali A, Bellina V, Resta F, Mariotti M, Massimini M (2009) Natural frequencies of human corticothalamic circuits. J Neurosci 29(24):7679–7685

Schadow J, Lenz D, Dettler N, Frund I, Herrmann CS (2009) Early gamma-band responses reflect anticipatory top-down modulation in the auditory cortex. Neuroimage 47(2):651–658. https://doi.org/10.1016/j.neuroimage.2009.04.074

Skosnik PD, Krishnan GP, O'Donnell BF (2007) The effect of selective attention on the gamma-band auditory steady-state response. Neurosci Lett 420(3):223–228. https://doi.org/10.1016/j.neulet.2007.04.072

Sohal VS, Zhang F, Yizhar O, Deisseroth K (2009) Parvalbumin neurons and gamma rhythms enhance cortical circuit performance. Nature 459(7247):698–702

Spencer KM, Salisbury DF, Shenton ME, McCarley RW (2008) Gamma-band auditory steady-state responses are impaired in first episode psychosis. Biol Psychiatry 64(5):369–375

Spencer KM, Niznikiewicz MA, Nestor PG, Shenton ME, McCarley RW (2009) Left auditory cortex gamma synchronization and auditory hallucination symptoms in schizophrenia. BMC Neurosci 10:85

Thanos PK, Robison L, Nestler EJ, Kim R, Michaelides M, Lobo MK, Volkow ND (2013) Mapping brain metabolic connectivity in awake rats with muPET and optogenetic stimulation. J Neurosci 33(15):6343–6349. https://doi.org/10.1523/JNEUROSCI.4997-12.2013

Thune H, Recasens M, Uhlhaas PJ (2016) The 40-Hz auditory steady-state response in patients with schizophrenia: a meta-analysis. JAMA Psychiatry 73(11):1145–1153. https://doi.org/10.1001/jamapsychiatry.2016.2619

Tiitinen H, Sinkkonen J, Reinikainen K, Alho K, Lavikainen J, Naatanen R (1993) Selective attention enhances the auditory 40-Hz transient response in humans. Nature 364(6432):59–60

Xu M, Chung S, Zhang S, Zhong P, Ma C, Chang WC, Weissbourd B, Sakai N, Luo L, Nishino S, Dan Y (2015) Basal forebrain circuit for sleep-wake control. Nat Neurosci 18(11):1641–1647. https://doi.org/10.1038/nn.4143

Yang C, Thankachan S, McCarley RW, Brown RE (2017) The menagerie of the basal forebrain: how many (neural) species are there, what do they look like, how do they behave and who talks to whom? Curr Opin Neurobiol 44:159–166. https://doi.org/10.1016/j.conb.2017.05.004

Zaborszky L, Csordas A, Mosca K, Kim J, Gielow MR, Vadasz C, Nadasdy Z (2013) Neurons in the basal forebrain project to the cortex in a complex topographic organization that reflects corticocortical connectivity patterns: an experimental study based on retrograde tracing and 3d reconstruction. Cereb Cortex. https://doi.org/10.1093/cercor/bht210